

Fast classical simulation of quantum circuits via parametric rewriting in the ZX-calculus

Matthew Sutcliffe  

Department of Computer Science, University of Oxford, Oxford, UK

Aleks Kissinger  

Department of Computer Science, University of Oxford, Oxford, UK

Abstract

The ZX-calculus is an algebraic formalism that allows quantum computations to be simplified via a small number of simple graphical rewrite rules. Recently, it was shown that, when combined with a family of “sum-over-Cliffords” techniques, the ZX-calculus provides a powerful tool for classical simulation of quantum circuits. However, for several important classical simulation tasks, such as computing the probabilities associated with many measurement outcomes of a single quantum circuit, this technique results in reductions over many very similar diagrams, where much of the same computational work is repeated. In this paper, we show that the majority of this work can be shared across branches, by developing reduction strategies that can be run parametrically on diagrams with boolean free parameters. As parameters only need to be fixed after the bulk of the simplification work is already done, we show that it is possible to perform the final stage of classical simulation quickly utilising a high degree of GPU parallelism. Using these methods, we demonstrate speedups upwards of 100x for certain classical simulation tasks vs. the non-parametric approach.

2012 ACM Subject Classification Theory of computation → Quantum computation theory; Computing methodologies → Parallel algorithms

Keywords and phrases Quantum computing, classical simulation / emulation of quantum computing, ZX-Calculus, graph rewriting, GPGPU

1 Introduction

The ZX-calculus [9, 26] is a useful tool for expressing a broad range of quantum computations, including quantum circuits, as a type of labelled graph called a *ZX-diagram*, and subsequently reducing it to a simpler form using a handful of graph rewriting rules. Recently, it has been applied extensively in optimisation [13, 11, 12, 3, 14, 20, 21] and classical simulation [17, 18, 27, 7, 8, 6, 19] of quantum circuits.

The latter application makes use of the fact that a single measurement amplitude associated with a quantum circuit can be represented as a ZX-diagram with no input/output wires. These closed diagrams semantically represent a 1×1 matrix, i.e. a scalar. While computing this scalar concretely may be hard in general, a seemingly very useful heuristic is to apply ZX-calculus rules to reduce the diagram as much as possible and only resort to more concrete calculations when the simplification gets stuck.

This rewriting-based technique terminates in polynomial time and provides some performance advantages over earlier methods for classical simulation of Clifford circuits [17], which have long been known to be efficiently classically simulable (see e.g. [1]). However, more interestingly, ZX-simplification can be combined with other classical simulation techniques to provide substantial advantages for heuristic simulations of non-Clifford circuits.

The work of Bravyi, Smith, and Smolin [5], as well as Bravyi et al [4], introduced the *sum-over-Cliffords* method for classical simulation of universal quantum circuits. In particular, the ‘BSS’ decomposition of [5] allows a set of 6 (computationally costly) T-gates to be exchanged for a sum of 7 (computationally cheap) Clifford terms. While this will still in general result in

an exponential blowup of terms, it improves on the naïve approach by a large constant factor, effectively more than doubling the size of circuits that can be feasibly classically simulated.

Kissinger and van de Wetering [17] showed how applying ZX-calculus reductions at every step of the decomposition leads to a significant reduction in the number of resulting diagrams, by allowing the costly T-gates to cancel wherever possible. With this approach, [17] and subsequently [18] showed an order-of-magnitude improvement over existing methods for random Clifford+T circuits, and substantially larger improvement for structured circuits.

However, a major disadvantage to this approach is that when multiple measurement amplitudes or probabilities are needed for the same circuit (e.g. when sampling the output distribution many times or computing marginal probabilities), the entire procedure needs to be repeated from the start to compute each amplitude. This makes certain classical simulation tasks infeasible for the existing ZX-based approach.

In this paper, we introduce a new simplification procedure for ZX-diagrams that allow boolean free parameters. Remarkably, the graph-theoretic simplification of such diagrams can be done in a way that is agnostic to the value of these parameters, which enables us to delay fixing them until near the end of the calculation. Ultimately, this allows – once the circuit has been reduced for the generalised case – for the respective results of different choices of free parameters to be calculated very rapidly, by simply evaluating a real-valued polynomial with boolean free variables. Furthermore, we show that such polynomials can be represented in such a way that these evaluations can be calculated in parallel on a GPU. Consequently, as the following sections will show, after the initial generalised reduction, every subsequent choice of parameters can be evaluated in a small fraction of the time that would be achieved by repeating the whole process.

2 Background

2.1 ZX-calculus

Quantum algorithms are commonly expressed graphically in the form of quantum circuit diagrams [23], which show the sequence of gates acting upon the qubits. A useful alternative notation is that of the ZX-calculus, wherein quantum computations are expressed as *ZX-diagrams* [10]. These are undirected, labelled graphs with distinguished inputs and outputs (depicted as “dangling wires”) and two different kinds of vertices, called *spiders*: namely *Z* (typically green or white) spiders, which are defined relative to the Z-axis of the Bloch sphere, and *X* (typically red or grey) spiders, which are defined relative to the X-axis. Each spider has also an associated *phase* (relating to the angle of rotation it induces), written either within the spider or alongside it (or omitted if it is zero). The Hadamard gate is also included, expressed as a box of typically yellow or white, though this may also be decomposed into *Z* and *X* spiders in accordance with the Euler decomposition rule (cf. Figure 3) [26]. An edge containing a Hadamard gate may also instead be expressed as a dashed blue line, known as a Hadamard edge.

Semantically, *Z*-spiders can be interpreted “generalised Z-phase gates”, which are $2^n \times 2^m$ matrices with a 1 in the top-left corner, $e^{i\alpha}$ in the bottom-right, and 0s elsewhere:

$$\left[\begin{array}{c:c} : & \alpha \\ \alpha & : \end{array} \right] = \begin{pmatrix} 1 & 0 & \cdots & 0 \\ 0 & 0 & \cdots & 0 \\ \vdots & \vdots & \ddots & \\ 0 & 0 & & e^{i\alpha} \end{pmatrix}$$

Similarly, X-spiders are generalised X-phase gates. One way to define them is by conjugating Z-spiders by Hadamard gates:

$$\begin{array}{c} \text{Diagram with a red circle containing } \alpha \text{ and two yellow squares} \\ \vdots \end{array} := \begin{array}{c} \text{Diagram with a green circle containing } \alpha \text{ and two yellow squares} \\ \vdots \end{array} \quad \text{where} \quad \llbracket \text{---} \square \text{---} \rrbracket = \frac{1}{\sqrt{2}} \begin{pmatrix} 1 & 1 \\ 1 & -1 \end{pmatrix}$$

More complex ZX-diagrams can be interpreted much like quantum circuits in terms of composition and tensor products of their components:

$$\begin{array}{c} \llbracket \begin{array}{c} \text{Diagram with } D \text{ and } E \\ \vdots \end{array} \rrbracket = \llbracket \begin{array}{c} \text{Diagram with } E \\ \vdots \end{array} \rrbracket \circ \llbracket \begin{array}{c} \text{Diagram with } D \\ \vdots \end{array} \rrbracket \\ \text{Diagram with } D \text{ and } E \\ \vdots \end{array} = \begin{array}{c} \llbracket \begin{array}{c} \text{Diagram with } D \\ \vdots \end{array} \rrbracket \otimes \llbracket \begin{array}{c} \text{Diagram with } E \\ \vdots \end{array} \rrbracket \\ \text{Diagram with } D \text{ and } E \\ \vdots \end{array}$$

and crossing wires are interpreted as “swap” gates: $\text{SWAP}(v \otimes w) = w \otimes v$. Whereas quantum circuits always describe unitary matrices, ZX-diagrams can in general be non-unitary. In particular, a ZX-diagram with m inputs and n outputs describes a $2^n \times 2^m$ matrix. If it has no inputs or outputs, it describes a $2^0 \times 2^0 = 1 \times 1$ matrix, i.e. a scalar. An important property of ZX-diagrams is that isomorphic graphs semantically describe the same linear map. This is sometimes stated as a “meta-rule” of ZX-calculus: *only connectivity matters*.

ZX-diagrams are universal, in the sense that any $2^n \times 2^m$ matrix over the complex numbers can be represented as a ZX-diagram, although in general it will be exponentially large. However, quantum circuits represented in most gatesets can be translated into ZX-diagrams with a constant overhead. In particular, CNOT, H, and Z-phase gates all have compact presentations as ZX-diagrams containing 1 or 2 generators.

ZX-calculus comes equipped with a number of *rewrite rules* that describe how certain structures within a ZX-diagram may be re-expressed as an equivalent (generally simplified) structure. Figure 1 shows the elementary rewrite rules. It should be noted that all rewrite rules still apply with all its spider colours inverted. The rules in Figure 1 are complete for *Clifford ZX-diagrams*, i.e. those diagrams whose angles are restricted to integer multiples of $\pi/2$ [2]. That is, for any Clifford diagrams D, E , if $\llbracket D \rrbracket = \llbracket E \rrbracket$, then D can be transformed into E using the rules in Figure 1. Extensions of these rules are known to be complete for all “Clifford+T” diagrams [15] (i.e. with phases $k\frac{\pi}{4}$ for $k \in \mathbb{Z}$) and all ZX-diagrams [22], but we will only need the rules in Figure 1 to derive our simplification procedure.

From the set of rules in Figure 1, there are also a number of *derived* rules. Two of particular interest in this paper are the *local complementation* and *pivoting* rules, shown in Figure 2. For a more comprehensive list of the rewrite rules, see e.g. [26].

Additionally, there is the Euler decomposition rule, which relates Hadamard gates/edges to Z- and X- spiders, and two types of fundamental scalar diagram components that may be exchanged in totality for scalar factors. These are outlined in Figure 3.

When restricted to the so-called *Clifford* gate-set, wherein every phase in the diagram is a multiple of $\pi/2$, scalar ZX-diagrams are very efficiently reducible. However, in introducing *T-gates* (or, more precisely, *T-like* gates) into the mix, this efficiency is lost. These gates correspond to spiders with phases of *odd* multiples of $\pi/4$. While some T-like gates may be liable to fuse and cancel, or be otherwise transferred from the diagram to the scalar factor (for instance via the state copy rule), many will typically hinder further simplification. When reaching such apparent dead-ends, however, one may continue the diagram’s reduction by decomposing the T-gates into sums of Cliffords.

The BSS decomposition, for instance (introduced in [5]) allows sets of 6 T-gates to be exchanged for sums of 7 Cliffords. As per [17], this can be expressed in ZX-calculus form

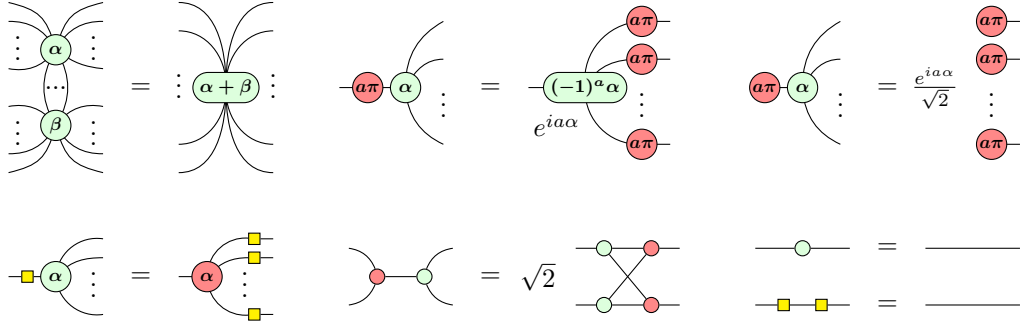


Figure 1 A set of the basic rewrite rules of ZX-calculus, where Greek letters denote arbitrary real variables, $[0, 2\pi)$, and Latin letters denote arbitrary boolean variables, $\{0, 1\}$. Note that the rules still apply if all the spider colours are inverted. These rules are known, in column-major order, as (a) spider fusion, (b) colour change, (c) π -commutation, (d) bialgebra, (e) state copy, (f) identity removal, and (g) Hadamard cancellation.

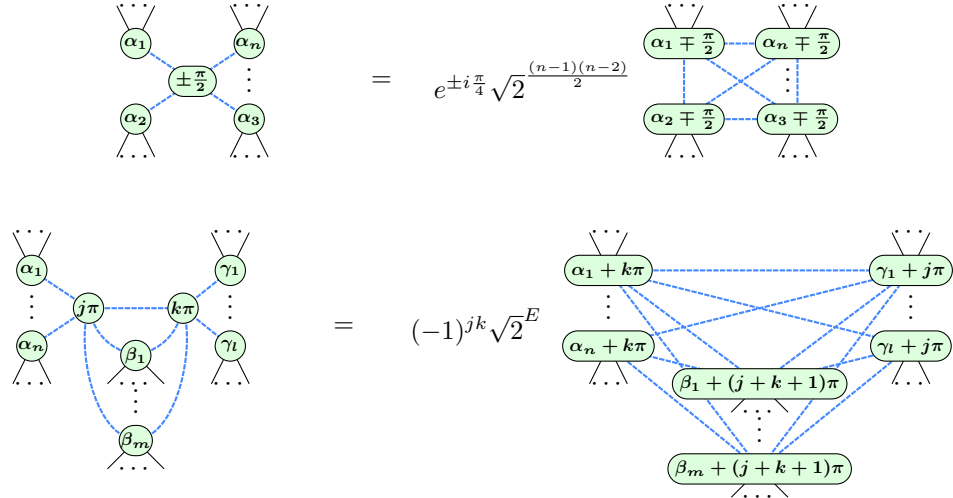


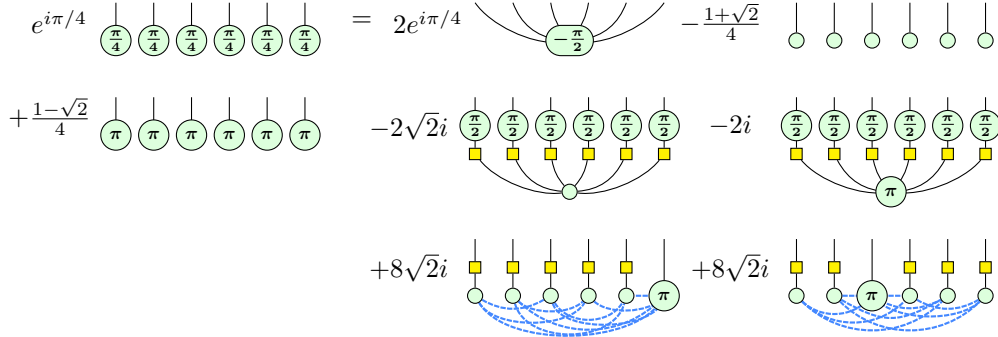
Figure 2 Two important derived ZX-calculus rewrite rules, namely (top) local complementation and (bottom) pivoting. Here, $E = (n-1)m + (l-1)m + (n-1)(l-1)$.

as in Figure 4. Consequently, utilising such a decomposition to remove T-gates, and hence allow the circuit to be further reduced, results in an exponential increase in the number of terms to compute (and correspondingly the runtime) versus the number of T-gates, t , in the initial simplified circuit. In the case of the BSS decomposition, this complexity is given by $7^{t/6} \approx 2^{0.47t}$. Hence, for a general decomposition complexity, $2^{\alpha t}$, BSS has an $\alpha \approx 0.47$ (where lower values of α represent more efficient decompositions). The current state of the art T-decompositions can achieve $\alpha \approx 0.396$ [24].

Furthermore, as explored in [17], at every stage of applying the decomposition to reduce the T-count (number of T-gates), the rewrite rules of ZX-calculus may be applied in order to, where possible, remove any T-gates that are now liable for removal. Given this extra step, the α values may be seen to represent, fairly naively, an estimate of the *upper-bound* of the number of terms that a Clifford+T circuit will decompose to.

$$\begin{aligned}
 \text{---} \square \text{---} &\equiv e^{-i\frac{\pi}{4}} \text{---} \circlearrowleft \frac{\pi}{2} \circlearrowright \frac{\pi}{2} \text{---} \equiv \text{-----} \\
 \textcircled{(\alpha)} = 1 + e^{i\alpha} \quad \textcircled{(\alpha)} \textcircled{(\alpha\pi)} &= \sqrt{2}e^{ia\alpha} \quad \textcircled{(\alpha)} \textcircled{(\beta)} = \frac{1}{\sqrt{2}}(1 + e^{i\alpha} + e^{i\beta} - e^{i(\alpha+\beta)}) \\
 \end{aligned}$$

■ **Figure 3** (Top) the Euler decomposition rule, relating a Hadamard gate to Z- and X- spiders, and (bottom) relations of fundamental scalar components (of which one is a special case of another), where $\alpha \in \mathbb{R}$ and $a \in \mathbb{B}$. These scalar components, together with the rewrite rules, are sufficient to reduce any scalar Clifford ZX-diagram into a numerical scalar and are respectively to be referred to as (left) *nodes* and (middle/right) *spider-pairs*.



■ **Figure 4** The BSS decomposition [5], relating a set of 6 T-gates to a sum of 7 Clifford terms, expressed in ZX-calculus terms as per [17].

2.2 Classical simulation

A very prominent task in the field is that of classically simulating quantum circuits, in order to, among other things, verify quantum algorithms and hardware. More specifically, this can be divided into *strong* and *weak* simulation, whereby the former is to deduce arbitrary (marginal) probabilities associated with specific measurement outcomes, while the latter is to produce sample outputs of a circuit in accordance with its output probability distribution.

As the name suggests, being able to perform strong simulation implies we can do weak simulation. However, this relies crucially on having access to marginal probabilities. Suppose one wishes to sample a bitstring (a_1, \dots, a_n) from the probability distribution associated with measuring the output of a quantum circuit. One can first compute the marginal probability $P(x_1 = 0)$, then set the first bit of the output $a_1 := 0$ with probability $P(x_1 = 0)$ and otherwise set $a_1 := 1$. We can compute the marginal probability $P(x_1 = a_1, x_2 = 0)$ and set the next bit $a_2 := 0$ with probability $P(x_1 = a_1, x_2 = 0)/P(x_1 = a_1)$ and set $a_2 := 1$ otherwise, and so on. Using the product rule, we see that the resulting bitstring will be sampled according to the distribution $P(x_1, \dots, x_n)$.

A circuit may be strongly simulated by plugging a fixed input state into the outputs and the conjugate-transpose of the state associated with a particular measurement outcome into the outputs. The resulting closed diagram can then be reduced to a single complex number λ via the means outlined in section 2.1. The quantity $|\lambda|^2$ then corresponds to the probability associated with that particular measurement outcome computed according to the Born rule of quantum theory. One may also deduce marginal probabilities, concerning measurement outcomes where some qubit outputs (a_1, \dots, a_k) are set, while not caring about the others (b_1, \dots, b_m) . Two means of denoting this in ZX-calculus (namely the ‘summing’ and ‘doubling’ approaches) are shown in Figure 5 [17]. As to which of these two options is more efficient varies from circuit to circuit, depending on a few factors, including the number of qubits and

how much cancellation is facilitated by partially composing against its own adjoint.

Both methods for computing marginal probabilities potentially incur an exponential overhead. The ‘summing’ approach requires summing over 2^m distinct terms, whereas the ‘doubling’ approach takes advantage of properties of the Born rule and ZX-diagrams to eliminate the sum, but doubles the size of the diagram, which for a Clifford+T circuit will double its T-count.

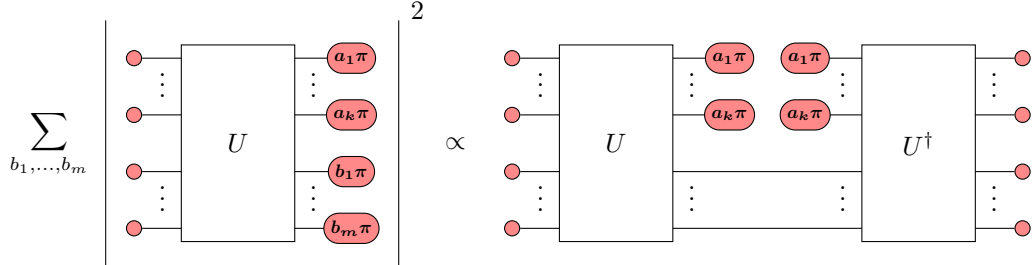


Figure 5 Two means of denoting as a ZX-diagram (up to a scalar factor) the probability that a circuit, U , will produce the qubit outcomes a_1, \dots, a_k , irrespective of the qubit outcomes b_1, \dots, b_m [17]. Note that $k + m = n$, for a circuit of n total qubits.

3 Method

3.1 Generalising ZX-calculus

The *Quizzx* [16] tool used for classical simulation of quantum circuits using the ZX-calculus in [17] and [18] does not support parameterised phases. That is to say every spider requires an exact numerical phase (such as $3\pi/2$, $\pi/4$, or 0), rather than some undefined symbolic variable (such as α or $\beta + \gamma/2$). The reason for this is that – as can be seen in Figures 1 and 2 – many of the rewrite rules require one or more of its spiders’ phases to take some specific value, or some value within a specific set. Take, for example, the *state copy* rule (see Figure 1). If both spiders on the left-hand side take unknown phases, α and β , then it remains unknown whether the rule may apply as it is undefined whether $\alpha \in \{0, \pi\}$ as required. As such, it must be assumed that the rule does not apply, since it does not *necessarily* do so. Likewise, the *local complementation* rule requires a spider of phase $\pm\pi/2$ and thus given an undefined symbolic phase, such as α , it would assume that the rule does not apply. While this same reasoning is not true of *all* the rules (*spider fusion*, for example, can always straightforwardly apply without any care for the phases involved), it is true of enough to prevent much practical simplification of parameterised (symbolically phased) graphs.

While this would be true of a *fully* generalised implementation of ZX-calculus, allowing any arbitrary parameterised phases (i.e. $\alpha, \beta, \gamma, \dots \in \mathbb{R}$), if instead the situation is appropriately restricted it can yield some useful results. In particular, this paper considers the case where all parameters are limited to booleans (i.e. $a, b, c, \dots \in \{0, 1\}$) and every parameterised term within a phase expression is limited to boolean multiples of π , meaning a phase of $\frac{\pi}{2} + a\pi + b\pi$ is allowed but $a\pi/2$ is not. Under these restrictions, the rewrite rules can (almost) all be maintained without loss of generality. One notable exception is the *identity removal* rule, which insists on a zero-phase spider, thus remaining ambiguous for a parameterised phase, $a\pi$. However, this rule is also exceptional in being a largely trivial one to the concerns here as they can be pushed aside and largely ignored.

We will initially consider the case of Clifford ZX-diagrams limited to integer multiples of

$\pi/2$, then proceed to considering the computationally universal set of Clifford+T diagrams toward the end of this section.

For Clifford ZX-diagrams, any ambiguity in a phase is always by a term of π . And as π amounts to half of a full rotation, any parameterised phase will always have two possible (and necessarily opposite) states. For instance, a phase of $a\pi$ may take only a value of 0 or $0 + \pi = \pi$ (i.e. $a\pi \in \{0, \pi\}$); a phase of $a\pi + b\pi + c\pi$ may also take only a value of 0 or $0 + \pi = \pi$ (i.e. $a\pi + b\pi + c\pi \in \{0, \pi\}$); and a phase of $\frac{\pi}{2} + a\pi + b\pi$ may take only a value of $\frac{\pi}{2}$ or $\frac{\pi}{2} + \pi = \frac{3\pi}{2}$ (i.e. $\frac{\pi}{2} + a\pi + b\pi \in \{\frac{\pi}{2}, \frac{3\pi}{2}\}$). The two possible states of any parameterised phase are thus always a pair of Clifford angles on opposite sides of the circle (i.e. $\{0, \pi\}$ or $\{\frac{\pi}{2}, \frac{3\pi}{2}\}$). Herein, the possible states a particular parameterised phase may take will be referred to as its *domain*. Note also that any phase will thus necessarily take the form of a sum of boolean parameters (or none) plus some Clifford constant: $a\pi + b\pi + \dots + \frac{n\pi}{2}$ (where $n \in \mathbb{Z}$).

It is due to the fact that the domain of any phase is always two opposite values on a circle (i.e. always separated by π) that the ambiguity remains a stable and nondisruptive one to the rewrite rules. Consider again the local complementation rule. While the central spider may take a parameterised (and hence ambiguous) phase, it will nevertheless always be known whether this rule applies. Either its domain is $\{0, \pi\}$, meaning the rule definitely does not apply, or it is $\{\pi/2, 3\pi/2\}$, meaning it definitely does. If indeed the rule does apply, then the ambiguity in this phase simply propagates through the rule. In the case of local complementation this becomes generalised as in Figure 6.

Figure 6 The local complementation rule, generalised for arbitrary parameterised phases that obey lemma 1. The new $e^{\mp i(\pi/2)(a \oplus b \oplus \dots)}$ factor in the scalar serves to conditionally ‘correct’ the sign of the exponent in the $e^{\pm i\pi/4}$ factor if $a \oplus b \oplus \dots = 1$. Note that \oplus is the binary *XOR* operation (i.e. addition modulo 2).

Most of the other rewrite rules can likewise be generalised quite straightforwardly by the same reasoning (as shown in appendix A), as any effect they have on a phase amounts to adding (or, equivalently, subtracting) π . The notable exception is the π -commutation rule, as this triggers a phase change of $\alpha \rightarrow -\alpha$ (rather than, say, $\alpha \rightarrow \alpha + \pi$). This can be easily resolved, however, by separating the rule into two distinct rules (one for $\alpha \in \{0, \pi\}$ and one for $\alpha \in \{\pi/2, 3\pi/2\}$), outlined in Figure 7. This essentially maps the central phase depending on its domain, $\{0, \pi\} \rightarrow \{0, \pi\}$ or $\{\frac{\pi}{2}, \frac{3\pi}{2}\} \rightarrow \{\frac{3\pi}{2}, \frac{\pi}{2}\}$, having the effect of always inverting the sign of the phase, by either adding nothing or adding π .

Having now justified that all of the important ZX-calculus simplification rules still apply to Clifford ZX-diagrams after introducing boolean parameters, it becomes worthwhile considering the impact of extending the gate-set to that of Clifford+T circuits. In this regime, every phase is given by the sum of zero or more boolean- π parameter terms ($a\pi + b\pi + c\pi + \dots$) plus some constant $k\pi/4$. As before, every parameter is strictly boolean ($a, b, c \in \{0, 1\}$) and every parameterised term strictly a boolean multiple of π (e.g. $a\pi/2$ is disallowed). This may be referred to as the ‘no ambiguous domains’ rule (lemma 1).

Figure 7 The π -commutation rule, separated into two distinct cases for the two possible domains of valid parameterised Clifford circuits. The left is applicable when commuting through a phase of $\{0, \pi\}$ domain and the right through a phase of $\{\pi/2, 3\pi/2\}$ domain. Both have the effect of flipping the sign of the phase, without violating lemma 1. Note that A and B here are shorthand for the XOR (addition modulo 2) sums of any amount (including zero) of boolean parameters: $A \equiv a_1 \oplus a_2 \dots \oplus a_i$ and $B \equiv b_1 \oplus b_2 \dots \oplus b_j$.

After extending the gate-set to allow $k\pi/4$ phases, the same logic as above can be applied to show that most of the rewrite rules can still remain generalised. For a given phase, such as $a\pi + c\pi + \pi/4$, one only needs to take note of the constant term to know whether or not a given rule applies. In this example, it is known that this phase can only equal $\pi/4$ or $5\pi/4$, depending on the values of a and c (which can each be 0 or 1). As such, its domain remains clearly known. Consequently, it is known that – for this phase – the local complementation rule, for instance, does not apply (as it requires a phase in the domain $\{\pi/2, 3\pi/2\}$).

The inconvenient exception, however, (aside from the largely trivial identity removal rule) is again the π -commutation rule. This rule cannot be generalised for the Clifford+T set without violating the no ambiguous domains rule (lemma 1). This is proven in Appendix B, Lemma 2. One may therefore conclude that ZX-calculus can be generalised in this fashion for Clifford circuits, but not for the wider Clifford+T set.

There is, however, a silver lining when applying this method to the Clifford+T set. Specifically, when dealing with scalar diagrams – that is, those with plugged inputs and outputs – the aim of simplification is to reduce the diagram fully to the complex scalar it represents. The rewrite strategies that achieve this do so via decomposition of the diagram's T-gates into a sum of Cliffords, as outlined in section 2.1. This means that Clifford+T scalar diagrams can be reduced to their final scalar form using only rewrite rules on Cliffords. In the simplest case, this would mean decomposing all T-gates in the original Clifford+T diagram to produce a large sum of Clifford diagrams which could then each be simplified to their scalar form, without ever needing to apply any rewrite rules to a T-like phase. This would allow the generalisation of parameterised ZX-calculus outlined above to be utilised without running into the issues that arise when T-like phases meet the π -commutation rule.

Better yet, one can simply proceed as normal with the Clifford+T scalar diagram reduction strategies – undergoing simplification on Clifford+T diagrams at each stage – *as far as possible*, while maintaining generality and simply forbidding the π -commutation rule (when ambiguous). Indeed, the particular strategy this paper considers is that of [17], which primarily relies on local complementation and pivoting (both of which – as has been shown above – remain reliable when generalised even for Clifford+T diagrams). In fact, the π -commutation rule does not interfere with the T-like spiders particularly often in this specific simplification strategy, and so while this approach can in principle result in considerably more summands at the end, in practise it seldom does.

This strategy, therefore, amounts to iteratively applying the parameterised set of rules, shown in Figure 10, in conjunction with the T-gate decomposition outlined in section 2.1 when no further simplification is possible with the rules.

Moreover, for reasons that will soon become apparent, the parameterised components of the scalars are isolated from the constant parts. For instance, applying the local complementation rule to a central spider of phase $a\pi + b\pi + \frac{\pi}{2}$ not only alters the ZX-diagram but also introduces a new scalar coefficient of $e^{i\pi(-1/2)(a+b)}e^{i\pi(1/4)}\sqrt{2}^{(n-1)(n-2)/2}$ (where n is defined as in Figure 6). This can be seen as the product of a parameterised component, $e^{i\pi(-1/2)(a+b)}$, and a constant component, $e^{i\pi(1/4)}\sqrt{2}^{(n-1)(n-2)/2}$. The constant part can be simply multiplied into the global scalar term of the ZX-diagram (which may be one among many summands, due to the T-gate decompositions). The *parameterised* component, meanwhile, may be added to a list of like components that apply to the present diagram. So, if the local complementation rule is collectively applied 4 times for various parameterised vertices in the diagram, then, along with simplifying the diagram and altering its constant scalar, it will also introduce 4 parameterised scalar factors, such as $e^{i\pi(-1/2)(a+b)} \cdot e^{i\pi(1/2)(b+c)} \cdot e^{i\pi(-1/2)(a+c)} \cdot e^{i\pi(1/2)(d+e+f)}$.

Each such parameterised scalar factor may be referred to as a *subterm*, while each individual scalar summand (reduced to a scalar from a ZX-diagram) – composed of the product of a number of subterms (including one constant factor subterm) – may be referred to as a *term*. In summary, with this terminology, one takes some initial scalar Clifford+T ZX-diagram and, via decompositions of the T-gates, expresses it as the sum of scalar Clifford ZX-diagrams. After exhaustively simplifying these diagrams, each reduces to simply a scalar *term*, being the product of parameterised (and one constant) *subterms*. So, each term is given by the product of its constituent subterms, and the final result is given by the sum of all terms. This structure is shown visually in Figure 8. Note that each term may have a different number of subterms (and these subterms themselves may be very different from one term to the next). Further note that if the original ZX-diagram were a Clifford one (as opposed to Clifford+T), then it would be described by just one term, made up of a number of subterms.

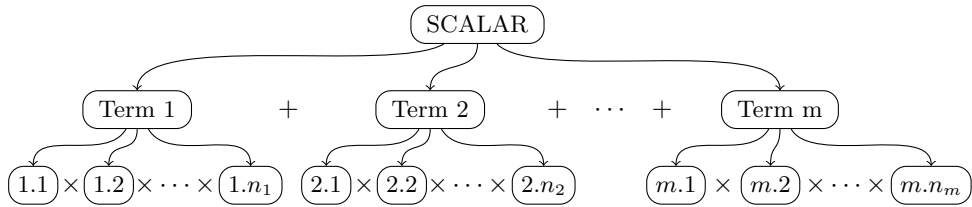


Figure 8 A breakdown of the structure of a parameterised scalar. A scalar Clifford+T ZX-diagram may be reduced to a parameterised scalar expression, comprised of a sum of *terms*, with each term being comprised of a product of some *subterms*.

In the examples above, it was shown that subterms of the form $e^{i\pi(\pm 1/2)(a+b+\dots)}$ arise whenever the local complementation rule is applied to a parameterised vertex. This is, however, just one type of subterm, which one may refer to as an *lcomp subterm* or a *half-pi subterm*. A small number of other distinct types of subterms may also arise; namely *node subterms*, *spider-pair* (or *phase-pair*) *subterms*, and lastly *pivot* (or *pi-pair*) *subterms*. These are summarised in table 1, highlighting their respective forms and origins.

After arriving at the generalised expression for a given circuit, to deduce the final result of the scalar for a particular set of inputs/outputs, one then need only substitute in values for the parameters (a, b, c, \dots) and evaluate the resulting terms. As a simple Clifford example, consider a ZX-diagram with parameterised inputs, $a\pi, b\pi, c\pi, d\pi, e\pi$. Supposing one wished to deduce the scalar this diagram represents for a given input, such as $a, b, c, d, e = (0, 0, 0, 0, 0)$,

| Name of Type | Form | Origin |
|--------------------------|--|---|
| Node | $(1 + e^{i\pi((C/4)+(a \oplus b \oplus \dots))})$ | Arise from standalone legless spiders (see Figure 10) |
| Spider-pair / phase-pair | $(1 + e^{i\pi A} + e^{i\pi B} - e^{i\pi A+B})$ | Arise from standalone pairs of connected spiders of opposite colour (see Figure 10) |
| lcomp / half-pi | $e^{i\pi(1/2)((C/4)+(a \oplus b \oplus \dots))}$ | Arise from applying the local complementation rule to a parameterised vertex (see Figure 6) |
| Pivot / pi-pair | $e^{i\pi(\frac{1}{4}C_1+(a_1 \oplus b_1 \oplus \dots))(\frac{1}{4}C_2+(a_2 \oplus b_2 \oplus \dots))}$ | Arise from applying the pivoting rule to a pair of vertices (of which at least one is parameterised), and the π -commutation rules (see Figures 7 and 10) |

■ **Table 1** The names, formulae, and origins of the different types of subterms. Here, A and B are shorthand for parameterised Clifford+T phases, $A := (a_1 \oplus b_1 \oplus c_1 \oplus \dots) + \frac{1}{4}C_1$ and $B := (a_2 \oplus b_2 \oplus c_2 \oplus \dots) + \frac{1}{4}C_2$. C , meanwhile, refers to the coefficient of the constant term, such that $C \in \{0, 1, 2, \dots, 7\}$. The choice of $C \in \{0, 4\}$ in the half-pi subterms is equivalent to selecting the \pm sign of the exponent in Figure 6 (and likewise for the pi-pair subterms).

traditionally they would substitute in these values ($a = 0, b = 0, \dots$) and then simplify the resulting (now non-parameterised) diagram. In the alternative approach offered by this paper, one could instead leave the original diagram in its parameterised form and simplify it to a parameterised scalar term (being the product of such subterms as in table 1) while maintaining generality. Only then would they be required to substitute in the desired parameter values ($a = 0, b = 0, \dots$) and evaluate the final result.

Now suppose one wished to find the scalar result of not just one but every (or at least many) possible combination of input values, for input states $\{0, \pi\}$, for the aforementioned example diagram. As this diagram takes 5 inputs (parameterised as $a\pi, b\pi, c\pi, d\pi, e\pi$), and each has two possible states (0 or π), then there are $2^5 = 32$ possible combinations of input values. In the traditional approach, this would require substituting in the values and simplifying the whole diagram 32 times to find all 32 results. In this alternative (parameterised) approach, it would require simplifying the original diagram just *once*, and subsequently evaluating the resulting parameterised scalar expression 32 times (once for each combination of parameter values).

At this stage, little (if any) speedup in computational runtime is offered, as evaluating some long complex expression with many subterms is comparably computationally costly as just simplifying the original diagram (hence 32 *evaluations* of the resulting parameterised scalar is roughly comparable in speed with 32 *simplifications* of the original diagram). The opportunity for significant speedup arises from the fact that, having reduced the diagram to a generalised (parameterised) scalar expression – whose terms all share the same restrictive set of forms/structures – it is now in a highly parallelisable state and requiring only very basic computation. That is to say, given the resulting parameterised expression denoting the scalar form of the diagram, all its possible evaluations for the various combinations of parameter values can be computed in parallel chunks, and only requiring very computationally cheap basic mathematical operations. Consequently, it is now in a form that lends itself very nicely to be processed on the GPU rather than the CPU.

3.2 Parallel evaluations on the GPU

With the data now in a highly parallelisable form, it remains to be structured in a computationally concise way that lends itself to efficient evaluation on the GPU. As such, the data can be translated into a primitive data structure, namely a simple set of two-dimensional arrays - one for each subterm type. Specifically, in each case, every row can record one such subterm by flagging which parameters are included (as well as recording any relevant constant), as per the type's form given by table 1.

Consider, for example, within a system of 4 parameters (a, b, c, d) , a very small scalar consisting of just two terms. Suppose the first term contains two node-type subterms, $(1+e^{i\pi((2/4)+(a\oplus b))})(1+e^{i\pi((4/4)+(b\oplus c\oplus d))})$, and the second contains just one, $(1+e^{i\pi((7/4)+(c))})$. The node-type subterm data for this scalar may then be represented as follows:

| * | C | a | b | c | d |
|---|-----|-----|-----|-----|-----|
| 1 | 2 | 1 | 1 | 0 | 0 |
| 1 | 4 | 0 | 1 | 1 | 1 |
| 1 | 7 | 0 | 0 | 1 | 0 |
| 0 | 0 | 0 | 0 | 0 | 0 |

The data for the other subterm types can be recorded likewise in similar arrays, with column headers based on table 1.

Note that dummy entries are included for padding where appropriate in order to ensure that, for each subterm type, each term has the same number of subterms. This further aids parallelism by simplifying indexing (as - in the above example case - the program can then recognise that every set of two rows corresponds to a term). A simple 'dummy flag' can be used to record whether each row is denoting a genuine subterm or just padding - as in the leftmost column above.

Moreover, to optimise for GPU parallelism even further, these 2D arrays are to be stored in memory in column-major order. This seemingly subtle point makes a huge difference to the computational runtime and a justification for this is detailed in appendix C.

Together with a few small pieces of relevant metadata (the number of parameters, terms, subterms per term etc.) and the constant factors of each term, the set of 2D arrays completely describe a parameterised scalar of the form outlined in section 3.1, in a concise manner that is efficiently structured for GPU computation.

With the data packaged in this way, it can be sent to the GPU, where it may be processed one array at a time, with each row being allocated its own thread (meaning the rows are processed in parallel). Thereupon, this data may be evaluated based on some set of parameter values (e.g. $a = 1, b = 0, c = 1, d = 0$) that are also to be sent to the GPU (though this amounts to a trivially small n bytes of data, given n parameters).

The subterm expressions may then be calculated very efficiently and in parallel, requiring only one or two bitwise dot products, followed by some basic arithmetic, and then a lookup table to return the respective numerical values from their phases. Appendix D outlines these steps more explicitly.

Lastly, as per Figure 8, these subterm rows may be multiplied as appropriate into their respective *terms*, and in turn these terms may be summed together to produce the final overall scalar result. Making one last use of GPU parallelism, these two steps may each be computed, via the algorithm outlined in appendix E, in up to $\log_2 n$ iterations (rather than n iterations as could be achieved on the CPU, by naïvely summing each term to the total in sequence), for n rows.

Note also that the multiplications and summations in these final steps may be calculated in a computationally efficient way by representing the complex expressions in the form $A + B\sqrt{2} + i(C + D\sqrt{2})$, where $A, B, C, D \in \mathbb{R}$. In this way, summation of such expressions is as simple as adding the like coefficients, while multiplication (e.g. against a running total $\alpha + \beta\sqrt{2} + i(\gamma + \delta\sqrt{2})$, where $\alpha, \beta, \gamma, \delta \in \mathbb{R}$) may be computed according to the following relations:

$$\begin{array}{ll} \alpha \rightarrow \alpha A + 2\beta B - \gamma C - 2\delta D & \beta \rightarrow \alpha B + \beta A - \gamma D - \delta C \\ \gamma \rightarrow \alpha C + 2\beta D + \gamma A + 2\delta B & \delta \rightarrow \alpha D + \beta C + \gamma B + \delta A \end{array}$$

The benefit of this approach is that, having initialised (and sent to the GPU) all the parameterised subterm matrices of the original parameterised scalar, one can re-evaluate it for a whole new set of parameter values very rapidly. As all the parameterised data remains sat on the GPU, to re-evaluate the scalar one simply needs to send to the GPU a new set of parameter values (e.g. $a = 1, b = 1, c = 0, d = 1$) and rerun the kernels. Since, after initialisation, the only data that is being sent for each new evaluation is simply a handful of bytes to input the parameter values and a handful of bytes to return the final result, the data transfer time for new evaluations is negligible. (This is especially true if one sends the data for the next evaluation while the present one is still computing - i.e. a pipelined approach.)

In conclusion, while initialising the parameterised data and sending it to the GPU (it may be several gigabytes and hence take a non-trivial time to transfer among the hardware) may be a relatively slow task, compared to conventionally computing the scalar of a Clifford+T ZX-diagram, once it is initialised one can evaluate the scalar for new sets of parameter values very quickly. This is because most of the work has already been done in the initialisation and all that remains is to substitute in the parameter values and simplify the result – and, more to the point, this is done in a highly parallelised manner. The upshot is that taking some Clifford+T scalar ZX-diagram and evaluating it for various sets of input parameter values is exceptionally quick with this method.

3.3 Application to classical simulation

Having now outlined a method by which a scalar Clifford+T quantum circuit may be reduced to its numerical scalar form, repeatedly for various sets of input values, it remains to showcase a useful application of this. One notable example is that of classical simulation of a quantum circuit (as described in section 2.2). Indeed, this paper’s method can be applied to this task in two different ways.

Firstly, one can apply this method to parallelise the summand calculations of the *summing* method of computing marginal probabilities (the left-hand side of Figure 5). As each summand corresponds to reducing the given circuit for a different set of boolean parameter values, it is clear to see that this paper’s method maps very directly to this application.

A second way the method can be applied to classical simulation is in optimising repeated weak classical simulation. The idea here is to produce samples of classically simulating a quantum circuit, many times. To do this using the methods above, the steps are much the same as those of section 2.2, with a new, doubled (and then simplified) graph being generated for each successive output qubit. The difference here is that, in each step, instead of fixing the preceding outputs based on the probabilities found in the previous steps, the graph can be doubled and reduced for the general, parameterised case (leaving the outputs as a, b, c, \dots). Then, this parameterised graph, corresponding to one specific qubit output, can be evaluated any arbitrary number of times very efficiently. Each result here can be kept as part of its own bitstring to pass onto the next qubit’s graph.

In summary, for a circuit of n qubits, this results in n distinct, parameterised graphs, generated one at a time. For each in succession, it may be evaluated r times (for r repeat simulations) to find the simulated output of the next qubit, for each of the r samples. Continuing this process for all qubits allows the original circuit to be classically simulated r times very efficiently – only ever needing to undergo the slow Clifford+T simplification routine on n Clifford+T graphs, rather than rn .

Note that circuits of very high T-count will produce parameterised scalars consisting of very many terms. As such, this data could in theory be many gigabytes and consequently exceed the storage capacity of the GPU. This could be easily rectified, however, by segmenting the data – structured as in Figure 8 – and processing it in parts via a depth-first approach.

4 Results

With this method, the runtime of each successive sample, after initialisation, is expected to be considerably quicker than that of the conventional approach, as it does not require redoing any simplifications. However, the initialisation involved in preparing the parameterised scalar and transmitting the data to the GPU means that it will take a number of samples before the *overall* runtime is improved by this approach. In other words, if only a few samples are taken then the overall runtime will be dominated by that of initialisation, whereas as the number of samples increases, this initialisation runtime becomes negligible to the overall runtime. As such, one important metric by which to measure the efficacy of the method is the theoretical maximum (or *terminal*) speedup it can offer for a given circuit (that being the speedup achieved as the number of samples approaches infinity and hence the initialisation time becomes negligible). This is simply given by the ratio of the runtime of one repeat sample in this new method vs that of the old method. In conjunction with this, it will be worthwhile to analyse how many samples are required for a significant improvement in runtime to be attained.

For a given example of a 36 T-gate circuit of 20 qubits, of which 5 are parameterised, the following result was measured. (Note that for all the experimental results that follow, the hardware used included a 6-core 2.69GHz Intel i5-11400H CPU and an 8GB NVIDIA GeForce GTX 1650 GPU.) The pre-existing Quizx tool [16] took 472ms to sample this circuit, whereas the new approach, after an initialisation time of 5.944s, required just 4.656ms (on average) to compute a sample. This gives a terminal speedup of $472/4.656 = 101.4$, meaning that, as the number of samples increases, this new method will run up to 101.4 times quicker than Quizx for computing those many samples. This is reflected in Figure 9a. Indeed, in this example, one need take only around 13 samples or more to see an improvement to the runtime. Better yet, as the graph shows, taking just thousands of samples gives a significant speedup (of at least 44x), and taking tens of thousands is sufficient to see speedups upwards of 90x. Note that while this shows an illustrative example, this pattern remains consistent among the other circuits measured.

The method outlined above was benchmarked against the more conventional, non-parameterised, approach of [17], for simplifying and taking many repeat evaluations of some random Clifford+T circuits. Such circuits of various T-counts were generated and exported from PyZX (based on its *generate.cliffordT* function). The terminal speedup factors (compared against Quizx) for these circuits are shown in Figure 9b, against their respective T-counts (after initial Clifford simplification).

As evidenced in this Figure, for small T-counts this method offers no notable speedup versus Quizx. This is to be expected as, given small T-counts, the number of resulting

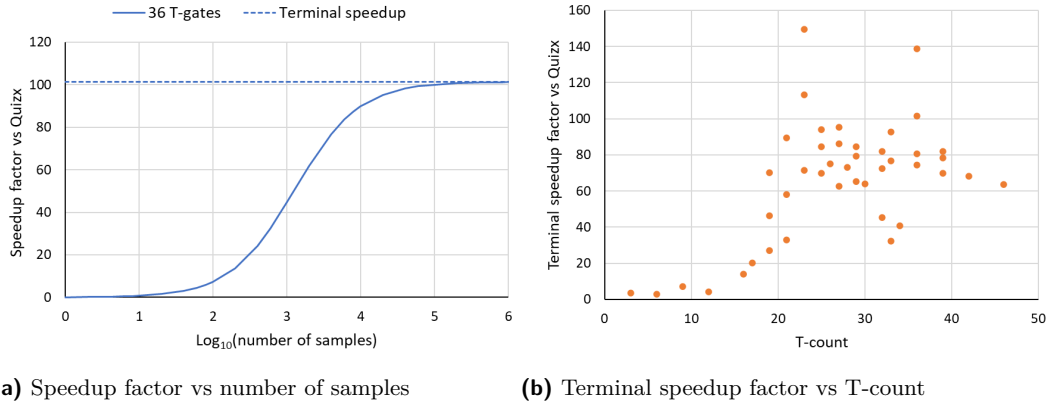


Figure 9 (a) The measured speedup factor, versus number of samples, for sampling a particular random 36 T-count circuit many times with the method outlined in this paper, as compared to the non-parameterised, non-parallelised conventional approach implemented in Quizx. (b) The experimental measurements of the *terminal* speedup factors (as compared, again, to the conventional Quizx approach) for random Clifford+T circuits of various T-counts.

terms is very small and hence is not able to take full advantage of the GPU parallelism (especially so if the number of terms is smaller than the number of parallel GPU threads). However, once the T-count is no longer trivially small, one can observe that this method is effective at providing speedups of up to, and even beyond, a factor of 100. Figure 9b shows a concentration of points between a speedup of 60x and 100x, largely irrespective of the T-count (beyond the trivially low cases), suggesting this is the typical improvement attained via this method (given the hardware specified). Though less common, there are also some extreme outliers among the non-trivial T-counts, highlighting speedups as high as 150x and as low as 32x.

It is important to emphasise that the effectiveness of this method varies from one ZX-diagram to another (even for the same T-count), depending on how well the diagram is able to reduce while maintaining generality. Owing largely to the problematic π -commutation rule, simplifying Clifford+T diagrams with evaluated phases will always result in fewer (or as many) scalar terms as simplifying the equivalent diagrams with some parameterised phases. So, the generalised approach will always end up with more scalar terms to compute. However, we observed that the generalised approach rarely resulted in more than 2x the total number of resulting scalar terms (and indeed was typically well below this). The effect of a mere doubling in the number of scalar terms to compute is more than counteracted by the ability of this method, with its use of the GPU, to compute them in bulk far quicker than the standard way.

Nevertheless, for the occasional unfortunate diagram that proves particularly ineffective at simplifying while maintaining generality, one may be left with 3 or more times the number of final scalar terms to compute than would have resulted from the non-generalised case. This usually occurs if the initial round of *Clifford* simplification (before any decomposition of the T-gates takes place) runs into π -commutation roadblocks that hinder generalised reduction of the T-gates. This, however, was observed to be relatively rare, on random circuits, but serves to explain the occasional lower-speedup outlier in Figure 9b. Conversely, the higher outliers can be explained as those circuits whose decompositions were very fortunate to be optimal, and to not be hindered by π -commutation roadblocks, at almost every instance.

Furthermore, the speed at which the GPU is able to compute many scalar terms depends

also on how many subterms are contained with them (and hence the number of calculations involved in evaluating each term). This in turn is determined by how many times pivoting and local complementation occur, as well as how many phase-nodes become separated from the their diagram, and so forth. This, however, was found to be fairly consistent and not a notable contributor to much fluctuation in the final speedup results measured.

It is worth noting that our approach doesn't depend on any particular structure of the BSS decomposition, so better decompositions could be adopted, such as those from [24], to obtain even more substantial improvements.

All of the relevant code for this project is hosted on Github [25]. This includes the modified PyZX code (to support parameterised reduction), further Python code to generate the GPU-ready datasets from the parameterised scalar data, as well as the CUDA code to evaluate these datasets on the GPU.

5 Conclusion and Future Directions

There are many applications in ZX-calculus where it is useful to compute (and often sum) many instances of the reduced scalar of a particular circuit, for various boolean input/output bitstrings. This paper highlights the redundancy inherent in such calculations and offers a mitigation of this redundancy. In particular, the paper shows how the quantum circuit reduction strategies of ZX-calculus can be parameterised, with appropriate considerations, to allow circuits to be reduced while maintaining arbitrary boolean inputs/outputs. In effect this means that instead of reducing a given circuit n times to compute its scalar for n different input/output bitstrings, one can instead reduce it just once (while maintaining generality), and thereafter simply *evaluate* the resulting parameterised expression n times.

Moreover, with this means of reducing a circuit to a generalised scalar expression, the paper then presents a method by which these n evaluations can be computed very efficiently via GPU parallelism, in a way that would not be feasible if dealing directly with graphical reductions. This was implemented in code and experimentally tested, and the observations showed that this approach was upwards of 100x quicker in computing many instances. This in turn can be interpreted as opening the door for larger quantum circuits (of greater T-counts) to be classically simulated in reasonable timeframes, as well as being applicable to a number of other related use-cases.

While not implemented within the scope of this paper, there are a number of small techniques that could be employed to further optimise the method outlined here. For instance, after a given circuit has been reduced to a parameterised scalar, there may often be many simplifications that could be applied to minimise the number of subterms involved. For example, node-type subterms that share the same set of parameters but whose constant terms differ by π may be cancelled pairwise in place of a constant, such as $(1 + e^{i\pi(\frac{2}{4} + (a \oplus b))})(1 + e^{i\pi(\frac{6}{4} + (a \oplus b))}) = (1 + e^{i\pi\frac{2}{4}})(1 + e^{i\pi\frac{6}{4}}) = (1 + i)(1 - i) = 2$. A special case of this is in cancelling such pairs whose constants are 0 and π respectively, as this reduces overall to 0, hence reducing the entire scalar term to 0, negating any need to compute it further. Minimising the number of subterms (and even terms) in this way would reduce the workload to compute when evaluating samples on the GPU, further improving runtime.

Furthermore, this paper primarily focused on applying the method outlined within to the use-case of classical simulation via the summing and/or doubling approaches. However, the method is a very general one, applicable to many related applications, such as breaking simulation tasks into disjoint components by node/wire-cutting [7] and performing weak simulation via the metropolis method described in [4].

References

- 1 Scott Aaronson and Daniel Gottesman. Improved simulation of stabilizer circuits. *CoRR*, quant-ph/0406196, 2004. URL: <http://arxiv.org/abs/quant-ph/0406196>.
- 2 Miriam Backens. The ZX-calculus is complete for stabilizer quantum mechanics. *New Journal of Physics*, 16(9):093021, 2014. doi:10.1088/1367-2630/16/9/093021.
- 3 Agustín Borgna, Simon Perdrix, and Benoît Valiron. Hybrid quantum-classical circuit simplification with the ZX-calculus. In Hakjoo Oh, editor, *Programming Languages and Systems*, pages 121–139, Cham, 2021. Springer International Publishing. doi:10.1007/978-3-030-89051-3_8.
- 4 Sergey Bravyi, Dan Browne, Padraig Calpin, Earl Campbell, David Gosset, and Mark Howard. Simulation of quantum circuits by low-rank stabilizer decompositions. *Quantum*, 3:181, 2019. doi:10.22331/q-2019-09-02-181.
- 5 Sergey Bravyi, Graeme Smith, and John A. Smolin. Trading classical and quantum computational resources. *Physical Review X*, 6(2):021043, 2016. doi:10.1103/PhysRevX.6.021043.
- 6 Tristan Cam and Simon Martiel. Speeding up quantum circuits simulation using ZX-Calculus. *arXiv preprint arXiv:2305.02669*, 2023.
- 7 Julien Codsí. Cutting-Edge Graphical Stabiliser Decompositions for Classical Simulation of Quantum Circuits. Master’s thesis, University of Oxford, 2022.
- 8 Julien Codsí and John van de Wetering. Classically Simulating Quantum Supremacy IQP Circuits through a Random Graph Approach. *arXiv preprint arXiv:2212.08609*, 2022.
- 9 Bob Coecke and Ross Duncan. Interacting quantum observables: categorical algebra and diagrammatics. *New Journal of Physics*, 13:043016, 2011. doi:10.1088/1367-2630/13/4/043016.
- 10 Bob Coecke and Aleks Kissinger. *Picturing Quantum Processes*. Cambridge University Press, 2017. doi:10.1017/9781316219317.
- 11 Alexander Cowtan, Silas Dilkes, Ross Duncan, Will Simmons, and Seyon Sivarajah. Phase Gadget Synthesis for Shallow Circuits. In Bob Coecke and Matthew Leifer, editors, *Proceedings 16th International Conference on Quantum Physics and Logic, Chapman University, Orange, CA, USA, 10-14 June 2019*, volume 318 of *Electronic Proceedings in Theoretical Computer Science*, pages 213–228. Open Publishing Association, 2020. doi:10.4204/EPTCS.318.13.
- 12 Niel de Beaudrap, Xiaoning Bian, and Quanlong Wang. Fast and Effective Techniques for T-Count Reduction via Spider Nest Identities. In Steven T. Flammia, editor, *15th Conference on the Theory of Quantum Computation, Communication and Cryptography (TQC 2020)*, volume 158 of *Leibniz International Proceedings in Informatics (LIPIcs)*, pages 11:1–11:23, Dagstuhl, Germany, 2020. Schloss Dagstuhl–Leibniz-Zentrum für Informatik. doi:10.4230/LIPIcs.TQC.2020.11.
- 13 Ross Duncan, Aleks Kissinger, Simon Perdrix, and John van de Wetering. Graph-theoretic Simplification of Quantum Circuits with the ZX-calculus. *Quantum*, 4:279, 6 2020. doi:10.22331/q-2020-06-04-279.
- 14 Stefano Gogioso and Richie Yeung. Annealing optimisation of mixed zx phase circuits. In Stefano Gogioso and Matty Hoban, editors, *Proceedings 19th International Conference on Quantum Physics and Logic, Wolfson College, Oxford, UK, 27 June - 1 July 2022*, volume 394 of *Electronic Proceedings in Theoretical Computer Science*, pages 415–431. Open Publishing Association, 2023. doi:10.4204/EPTCS.394.20.
- 15 Emmanuel Jeandel, Simon Perdrix, and Renaud Vilmart. A Complete Axiomatisation of the ZX-Calculus for Clifford+T Quantum Mechanics. In *Proceedings of the 33rd Annual ACM/IEEE Symposium on Logic in Computer Science*, LICS ’18, pages 559–568, New York, NY, USA, 2018. ACM. doi:10.1145/3209108.3209131.
- 16 Aleks Kissinger and John van de Wetering. Quizx. URL: <https://github.com/Quantomatic/quizx>.
- 17 Aleks Kissinger and John van de Wetering. Simulating quantum circuits with zx-calculus reduced stabiliser decompositions. *Quantum Science and Technology*, 7(4):044001, 2022. doi:10.1088/2058-9565/ac5d20.

- 18 Aleks Kissinger, John van de Wetering, and Renaud Vilmar. Classical Simulation of Quantum Circuits with Partial and Graphical Stabiliser Decompositions. In François Le Gall and Tomoyuki Morimae, editors, *17th Conference on the Theory of Quantum Computation, Communication and Cryptography (TQC 2022)*, volume 232 of *Leibniz International Proceedings in Informatics (LIPIcs)*, pages 5:1–5:13, Dagstuhl, Germany, 2022. Schloss Dagstuhl – Leibniz-Zentrum für Informatik. doi:10.4230/LIPIcs.TQC.2022.5.
- 19 Mark Koch, Richie Yeung, and Quanlong Wang. Speedy Contraction of ZX Diagrams with Triangles via Stabiliser Decompositions. *arXiv preprint arXiv:2307.01803*, 2023.
- 20 Tommy McElvanney and Miriam Backens. Flow-preserving ZX-calculus Rewrite Rules for Optimisation and Obfuscation. In Shane Mansfield, Benoit Valiron, and Vladimir Zamzhiev, editors, *Proceedings of the Twentieth International Conference on Quantum Physics and Logic, Paris, France, 17-21st July 2023*, volume 384 of *Electronic Proceedings in Theoretical Computer Science*, pages 203–219. Open Publishing Association, 2023. doi:10.4204/EPTCS.384.12.
- 21 Maximilian Nägele and Florian Marquardt. Optimizing ZX-Diagrams with Deep Reinforcement Learning. *arXiv preprint arXiv:2311.18588*, 2023.
- 22 Kang Feng Ng and Quanlong Wang. Completeness of the ZX-calculus for Pure Qubit Clifford+T Quantum Mechanics. *arXiv:1801.07993*, 1 2018.
- 23 Michael A. Nielsen and Isaac L. Chuang. *Quantum Computation and Quantum Information*. Cambridge University Press, 2010. doi:10.1017/CBO9780511976667.
- 24 Hammam Qassim, Hakop Pashayan, and David Gosset. Improved upper bounds on the stabilizer rank of magic states. *Quantum*, 5:606, December 2021. doi:10.22331/q-2021-12-20-606.
- 25 Matthew Sutcliffe. Paramzx. URL: <https://github.com/mjsutcliffe99/ParamZX>.
- 26 John van de Wetering. Zx-calculus for the working quantum computer scientist. 2020. URL: <https://api.semanticscholar.org/CorpusID:229680014>.
- 27 Robert Wille, Lukas Burgholzer, Stefan Hillmich, Thomas Grurl, Alexander Ploier, and Tom Peham. The Basis of Design Tools for Quantum Computing: Arrays, Decision Diagrams, Tensor Networks, and ZX-Calculus. In *Proceedings of the 59th ACM/IEEE Design Automation Conference, DAC '22*, page 1367–1370, New York, NY, USA, 2022. Association for Computing Machinery. doi:10.1145/3489517.3530627.

A Generalised Rewrite Rules

The rewrite rules of ZX-calculus, outlined in Figures 1 and 2, can be generalised to support symbolic Clifford+T phases of the form $a\pi + b\pi + c\pi + \dots + n\frac{\pi}{4}$ (where $a, b, c, \dots \in \mathbb{B}$ and $n \in \{0, 1, 2, \dots, 7\}$), as shown collectively among Figures 6, 7, and 10. (The remaining rules require no change to generalise and remain consistent with the forms outlined in 1.) It is important to note that these rules have been generalised to support parameterised spiders and these parameters are appropriately absorbed into the scalars when the rules are applied. Moreover, the standard rules (Figures 1 and 2) and scalars (Figure 3) are still applicable when no parameters are directly involved (though these do not introduce any parameterised subterms but rather may simply modify the term constants).

$$\begin{aligned}
 \text{Top: } & (A\pi + \frac{n\pi}{4}) = 1 + e^{i\pi(A + \frac{n}{4})} \\
 \text{Second: } & (A\pi + \frac{n\pi}{4}) - (B\pi + \frac{m\pi}{4}) = \frac{1}{\sqrt{2}}(1 + e^{i\pi(A + \frac{n}{4})} + e^{i\pi(B + \frac{m}{4})} - e^{i\pi(A + B + \frac{n+m}{4})}) \\
 \text{Third: } & \begin{array}{c} \text{---} \\ \text{---} \\ \text{---} \\ \vdots \\ \text{---} \end{array} \quad = \frac{1}{\sqrt{2}}e^{iA\alpha} \quad \begin{array}{c} \text{---} \\ \text{---} \\ \text{---} \\ \vdots \\ \text{---} \end{array} \\
 \text{Bottom: } & \begin{array}{c} \text{---} \\ \text{---} \\ \text{---} \\ \vdots \\ \text{---} \end{array} \quad = (-1)^{AB} \sqrt{2}^E \quad \begin{array}{c} \text{---} \\ \text{---} \\ \text{---} \\ \vdots \\ \text{---} \end{array}
 \end{aligned}$$

Figure 10 Generalisations of (top to bottom) the free node scalar, the spider pair scalar, the state copy rule, and the pivoting rule, to support parameterised phases, where $A \equiv a_1 \oplus a_2 \dots \oplus a_i$ and $B \equiv b_1 \oplus b_2 \dots \oplus b_j$. Care should be taken to distinguish between \oplus and $+$ in the exponents.

B Theorems and Lemmas

► **Lemma 1** (No ambiguous domains rule). *To allow for consistently-structured generalised ZX-diagram reduction (π -commutation and identity removal rules excluded), all phases must have non-ambiguous domains, each being either an exact value or a set of two opposite (separated by π) possibilities. That is to say, every phase must be expressible as the sum of some (or none) boolean- π parameterised terms (e.g. $a\pi + b\pi + c\pi + \dots$) plus some constant. Fractional coefficients on parameterised terms (e.g. $a\pi/2$) are thus disallowed within the graphs (but are allowed within any scalar factors).*

Proof. If a phase is expressible as a sum of boolean- π parameters plus some constant, C , then its domain will be strictly known as a set of two opposite possibilities (separated by π), namely $\{C, C + \pi\}$. As such, all the rewrite rules (aside from π -commutation and the trivial identity removal) may apply, or not apply, with certainty, based on the constant, with the parameterised component contributing to some scalar. However, introducing a fractional

coefficient to a parameter within a phase, such as $a\pi/2$, results in a more ambiguous domain, whose possible phases are *not* separated by π , and by extension this leads to ambiguity as to whether some rules may apply (namely the all important local complementation and pivoting rules). \blacktriangleleft

► **Lemma 2.** *The π -commutation rule cannot be generalised for the Clifford+T set while maintaining consistent graph structure.*

Proof. To generalise the π -commutation rule for the Clifford+T set, it would have to be separated into 4 distinct cases (applying to the different options of domain for the central spider's phase). The problem here is that, given a non-Clifford phase in the central spider, the difference in the result of applying the rule for a phase given one set of parameter values versus another cannot be expressed generally with a conditional $+\pi$ phase. For instance, if the central phase were $\pi/4$ and one wished to commute a spider of phase $a\pi$ through it, then the rule would need to map the former to $\pi/4 \rightarrow \pi/4$ if $a = 0$ and $\pi/4 \rightarrow -\pi/4$ if $a = 1$. However, the latter of these mappings corresponds to a change of phase of $\pi/2$, and as such this would necessarily have to be generalised as: $\pi/4 \rightarrow \pi/4 - a\pi/2$. Rather problematically, this violates the no ambiguous domains rule (lemma 1), by introducing a fractional parameter term into a phase (in this case $a\pi/2$).

To see why this is a problem, consider a spider of phase $a\pi/2 + b\pi/2 + c\pi/2$. The domain of this phase is no longer confined to two opposite points on a circle. In fact, in this case, its domain includes 4 possible states: $\{0, \frac{\pi}{2}, \pi, \frac{3\pi}{2}\}$, depending on the values of its parameters. Consequently, one cannot say with certainty whether, for example, the local complementation rule may apply. Thus, the rule cannot be neatly generalised in a way that maintains consistent graph structure. \blacktriangleleft

C A Justification for Column-Major Ordering

Consider a scalar of 4 parameters (a, b, c, d) consisting of three terms. The node-type subterm data for this scalar may be recorded like so:

| * | C | a | b | c | d |
|---|-----|-----|-----|-----|-----|
| 1 | 2 | 1 | 1 | 0 | 0 |
| 1 | 4 | 0 | 1 | 1 | 1 |
| 0 | 0 | 0 | 0 | 0 | 0 |
| 1 | 6 | 1 | 0 | 1 | 0 |
| 0 | 0 | 0 | 0 | 0 | 0 |
| 0 | 0 | 0 | 0 | 0 | 0 |
| 1 | 5 | 0 | 0 | 0 | 1 |
| 1 | 0 | 1 | 1 | 0 | 1 |
| 1 | 2 | 0 | 0 | 1 | 0 |

For each row (subterm) here, the parameters, a, b, c, d , and constant, C , are corresponding to the node-type formula outlined in table 1. The additional column on the left is the *dummy flag*, set to 1 if the row is recording a genuine subterm and 0 if it is instead a dummy row for padding (which may be ignored). So, the first three rows here correspond to the node-type subterm data for the first term, and the next three rows likewise for the next term, and the last three rows for the third term.

While for practical purposes this data is treated as two-dimensional, as far as the memory is concerned it is in fact, necessarily stored linearly. Conventionally, this would be stored,

linearised, in row-major order (storing the cells of the first row, followed by those of the second row and so on). This is appropriate when the data is to be processed row-by-row on the CPU (whose processing pattern is inherently sequential), as each subsequent element of data to be processed is stored immediately after the previous, ensuring convenient (quicker) access.

However, if instead, as in this case, each row of this data is to be processed in parallel on the GPU, then this memory arrangement proves to be suboptimal. In this scenario, it is preferential to store the data in column-major order (meaning all the cells of the first column are stored one after the other, followed then by the cells of the second column and so on). A justification for this follows:

► **Lemma 3.** *To better optimise for GPU processing, the two-dimensional subterm data should be stored in memory in column-major order (rather than the more typical row-major order that 2D arrays tend to be stored as).*

Proof. When the rows are to be processed in parallel, they will process their respective *dummy flags* (their data of the first column) at the same time, and then their respective *constant factors* (the second column) at the same time, and so on. Consequently, storing all the *dummy flags* (the first column) together in memory means that they can all be retrieved very efficiently, with many being moved in one go (as opposed to individually locating and sending each row's dummy flag one by one). For this reason, the two-dimensional data of the node-type subterms (and likewise for the 2D arrays of other subterm types) is better stored in column-major order, for a far more efficient ('*coalesced*') memory access pattern. ◀

D GPU Evaluation Method

Given the data for a parameterised scalar (formulated into a set of 2D arrays as described in section 3.2), the process to evaluate it for a particular set of parameter values can be computed very efficiently in a parallelised manner on the GPU. Firstly, these parameter values may be substituted into every subterm expression (in parallel) via a simple bitwise multiplication. The following table shows an example of this, whereby the parameter values $(a, b, c, d) = (1, 0, 1, 0)$ are multiplied into each row of some sample node-type subterm data.

This amounts to substituting in the parameter values for each subterm expression. In the first row of the example, this effectively means: $(1 + e^{i\pi((2/4)+(a \oplus b))}) \rightarrow (1 + e^{i\pi((2/4)+(1 \oplus 0))})$.

Next, the XOR strings within each exponential may be evaluated quite straightforwardly via basic arithmetic, providing a value of 0 or 1 for each row (computed, again, in parallel). In the first row example, this means reducing the XOR string, $1 \oplus 0 \rightarrow 1$, taking the result to: $(1 + e^{i\pi((2/4)+(1 \oplus 0))}) \rightarrow (1 + e^{i\pi((2/4)+(1))})$.

If the result of this reduced XOR string is labelled x , then it may be added to its neighbouring constant (while keeping a $1/4$ factor to maintain integer data types), like so: $y = C + 4x$ (modulo 8). This is equivalent to the step: $(1 + e^{i\pi((2/4)+1)}) \rightarrow (1 + e^{i\pi(6/4)})$, where $y = 6$.

Finally, these expressions are ready to be simplified fully. To avoid intensive calculations involving complex exponentials, a shortcut may be used. Considering that there are only 8 possible outcomes for each row ($y \in \{0, 1, \dots, 7\}$), and that the resulting complex numbers may be each expressed with 4 real numbers, $(1 + e^{i\pi(y/4)}) \equiv A + B\sqrt{2} + i(C + D\sqrt{2})$, the following lookup table may be used to map each row to its final result based on its constant, y .

Taking again the example subterm (where $y = 6$), this then reduces to $(1 + e^{i\pi(6/4)}) \rightarrow 1 + 0\sqrt{2} + i(-1 + 0\sqrt{2})$, which is recorded as 4 numbers, $(A, B, C, D) = (1, 0, -1, 0)$.

| * | C | a | b | c | d |
|----------|-----|-----|-----|-----|-----|
| 1 | 1 | 1 | 0 | 1 | 0 |
| \times | | | | | |
| * | C | a | b | c | d |
| 1 | 2 | 1 | 1 | 0 | 0 |
| 1 | 4 | 0 | 1 | 1 | 1 |
| 0 | 0 | 0 | 0 | 0 | 0 |
| 1 | 6 | 1 | 0 | 1 | 0 |
| 0 | 0 | 0 | 0 | 0 | 0 |
| 0 | 0 | 0 | 0 | 0 | 0 |
| 1 | 5 | 0 | 0 | 0 | 1 |
| 1 | 0 | 1 | 1 | 0 | 1 |
| 1 | 2 | 0 | 0 | 1 | 0 |
| $=$ | | | | | |
| * | C | a | b | c | d |
| 1 | 2 | 1 | 0 | 0 | 0 |
| 1 | 4 | 0 | 0 | 1 | 0 |
| 0 | 0 | 0 | 0 | 0 | 0 |
| 1 | 6 | 1 | 0 | 1 | 0 |
| 0 | 0 | 0 | 0 | 0 | 0 |
| 0 | 0 | 0 | 0 | 0 | 0 |
| 1 | 5 | 0 | 0 | 0 | 0 |
| 1 | 0 | 1 | 0 | 0 | 0 |
| 1 | 2 | 0 | 0 | 1 | 0 |

| y | A | B | C | D |
|-----|-----|------|-----|------|
| 0 | 2 | 0 | 0 | 0 |
| 1 | 1 | 1/2 | 0 | 1/2 |
| 2 | 1 | 0 | 1 | 0 |
| 3 | 1 | -1/2 | 0 | 1/2 |
| 4 | 0 | 0 | 0 | 0 |
| 5 | 1 | -1/2 | 0 | -1/2 |
| 6 | 1 | 0 | -1 | 0 |
| 7 | 1 | 1/2 | 0 | -1/2 |

Recall that the steps above are processed for each row in parallel. Along with the shortcuts described, this makes for a very efficient means of evaluating all the subterms. All that remains from this stage is to multiply together every set of 3 consecutive rows (that is in this example, where each term contains 3 subterms) to find the results of every *term*, before finally summing together all these term expressions (see Figure 8). These last two steps may also be computed in an efficient and parallelised manner, via the method outlined in appendix E.

E Parallelised Summation Algorithm

Given an array of n numbers, the best method for summing (or alternatively multiplying) all its elements - via sequential (i.e. single-core CPU) computation - is to simply iterate linearly through the whole array while maintaining a total tally. This gives a runtime complexity of $O(n)$.

Alternatively, by instead processing the data on the GPU, one may compute such a calculation while taking advantage of parallelism. Consider, for example, the following 10-element array:

$$[0, 1, 2, 3, 4, 5, 6, 7, 8, 9]$$

One can allocate a single GPU thread for every adjacent pair of elements. For the general case of an n -element array, this means allocating $n/2$ threads, which in this example case means 5 threads, divided as follows:

$$[\mathbf{0}, 1, \mid \mathbf{2}, 3, \mid \mathbf{4}, 5, \mid \mathbf{6}, 7, \mid \mathbf{8}, 9]$$

Each thread, running in parallel, may then sum the two elements under its consideration and overwrite its left element with the result, like so:

$$[\mathbf{1}, 1, \mid \mathbf{5}, 3, \mid \mathbf{9}, 5, \mid \mathbf{13}, 7, \mid \mathbf{17}, 9]$$

The right element of each pair can hereafter be ignored and so is written in grey here. The process can then repeat - this time with $n/4$ threads being allocated to consider, respectively, adjacent groups of 4 elements, like so:

$$[\mathbf{1}, 1, 5, 3, \mid \mathbf{9}, 5, 13, 7, \mid \mathbf{17}, 9]$$

Now, for each thread, the leftmost element will be incremented by the value contained 2 elements to its right (unless that index exceeds the length of the array):

$$[\mathbf{6}, 1, 5, 3, \mid \mathbf{22}, 5, 13, 7, \mid \mathbf{17}, 9]$$

This process then repeats iterative, halving the number of threads needed each time and doubling, for each thread, the number of elements considered and the gap between its relevant elements. This procedure follows as such:

$$[\mathbf{6}, 1, 5, 3, 22, 5, 13, 7, \mid \mathbf{17}, 9]$$

$$[\mathbf{28}, 1, 5, 3, 22, 5, 13, 7, \mid \mathbf{17}, 9]$$

$$[\mathbf{28}, 1, 5, 3, 22, 5, 13, 7, 17, 9]$$

$$[\mathbf{45}, 1, 5, 3, 22, 5, 13, 7, 17, 9]$$

Once the segment size exceeds the length of the array, the procedure is complete and the final result (in this case 45) - being the sum of all the elements in the original array - is stored in the first element.

Theoretically, this method computes in as few as $\log_2 n$ iterations, rather than n . Realistically, however, as the number of threads on a GPU is finite, for sufficiently large arrays the theoretically parallelised steps won't all occur simultaneously but rather in locally parallelised batches. Nevertheless, even as $n \rightarrow \infty$ this method requires significantly fewer iterations than

the naïve approach. And lastly, note that the method also works likewise for multiplication as well as summation.

The pseudocode for this method is provided in algorithm 1, where the *PSum* procedure computes in parallel on n threads - with each given a successive thread index provided by *GetThreadIndex()*.

This algorithm (or variations thereof) is used as described in the paper, for both multiplying the subterms within each term as well as summing all the terms in the overall scalar. The only major difference to note is that instead of the simple number summing calculation on line 7, the complex numbers are summed (and later multiplied) according to the relations outlined in section 3.2.

■ **Algorithm 1** The GPU-parallelised summation algorithm

```

1: Initialise and populate  $ARR[N_{ELEMS}]$   $\triangleright$  The array whose elements are to be summed
2:
3: procedure PSUM( $split, gap$ ) $<< n >>$   $\triangleright$  This is a GPU kernel, executing on  $n$  threads
4:    $i \leftarrow \text{GETTHREADIDX}()$   $\triangleright$  This function returns the unique thread index
5:    $elem \leftarrow i \times split$ 
6:   if  $elem + gap < N_{ELEMS} - 1$  then
7:      $ARR[elem] \leftarrow ARR[elem] + ARR[elem + gap]$ 
8:   end if
9: end procedure
10:
11:  $split \leftarrow 2$ 
12:  $gap \leftarrow 1$ 
13: while  $gap < N_{ELEMS}$  do
14:    $n_{chunks} \leftarrow \lceil N_{ELEMS} / split \rceil$ 
15:   PSUM( $split, gap$ ) $<< n_{chunks} >>$ 
16:    $split \leftarrow split \times 2$ 
17:    $gap \leftarrow gap \times 2$ 
18: end while

```
